Inorganic Chemistry

Article

pubs.acs.org/IC

Novel Heterometallic Schiff Base Complexes Featuring Unusual Tetranuclear $\{Co^{III}_2Fe^{III}_2(\mu\text{-}O)_6\}$ and Octanuclear $\{Co^{III}_4Fe^{III}_4(\mu\text{-}O)_{14}\}$ Cores: Direct Synthesis, Crystal Structures, and Magnetic Properties

Eduard N. Chygorin,[†] Oksana V. Nesterova,*[,†] Julia A. Rusanova,[†] Vladimir N. Kokozay,[†] Volodymyr V. Bon,[‡] Roman Boča,[§,⊥] and Andrew Ozarowski[¶]

[†]Department of Inorganic Chemistry, National Taras Shevchenko University, Volodymyrska street 64, Kyiv 01601, Ukraine

[‡]Department of Chemistry of Complex Compounds, V. I. Vernadsky Institute of General and Inorganic Chemistry, National Academy of Sciences of Ukraine, 32/34 Palladin Avenue, Kyiv 03680, Ukraine

[§]Department of Chemistry, FPV, University of SS Cyril and Methodius, Trnava, Slovakia

[⊥]Institute of Inorganic Chemistry, FCHPT, Slovak University of Technology, Radlinskeho 9, 81237 Bratislava, Slovakia

[¶]National High Magnetic Field Laboratory, Florida State University, 1800 E. Paul Dirac Drive, Tallahassee, Florida 32310, United States

Supporting Information

ABSTRACT: A one-pot reactions of cobalt powder with iron(II) chloride in dimethylformamide (DMF; **1**) or dimethyl sulfoxide (DMSO; **2**) solutions of polydentate salicylaldimine Schiff base ligands (H_2L^1, **1**; H_4L^2, **2**) based on 2-aminobenzyl alcohol (**1**) or tris(hydroxymethyl)aminomethane (**2**), formed in situ, yielded two novel heterometallic complexes, $[Co^{III}_2Fe^{III}_2(L^1)_6]\cdot 4DMF$ (**1**) and $[Co^{III}_4Fe^{III}_4(HL^2)_8(DMSO)_2]\cdot 18DMSO$ (**2**). Crystallographic investigations revealed that the molecular structure of **1** is based on a tetranuclear core, $\{Co^{III}_2Fe^{III}_2(\mu\text{-}O)_6\}$, with a chainlike metal arrangement, while the structure of **2** represents the first example of a heterometallic octanuclear core, $\{Co^{III}_4Fe^{III}_4(\mu\text{-}O)_{14}\}$, with a quite rare manner of metal organization, formed by two pairs of $\{CoFe(HL^2)_2\}$ and $\{CoFe(HL^2)_2(DMSO)\}$ moieties, which are joined by O bridges of the Schiff base ligands. Variable-temperature (1.8−300 K) magnetic susceptibility measurements showed a decrease of the μ_B value at low temperature, indicative of antiferromagnetic coupling ($J/hc = -32$ cm^{-1} in **1**; $J/hc = -20$ cm^{-1} in **2**) between the Fe^{III} magnetic centers in both compounds. For **2**, three J constants between Fe^{III} centers were assumed to be identical. High-frequency electron paramagnetic resonance spectra allowed one to find spin Hamiltonian parameters in the coupled-spin triplet and quintet states of **1** and estimate them in **2**. The "outer" and "inner" Fe atoms in **2** appeared separately in the Mössbauer spectra.

INTRODUCTION

The high-nuclearity transition-metal complexes represent an extremely actively pursued topic in modern coordination chemistry, reflecting the fact that polynuclear clusters are relevant to many different areas of science, including chemistry, biology, and solid-state physics. Furthermore, high-nuclearity solids are also attractive from the crystallographic point of view because they are able to reveal a wide range of shapes and different manners of metal arrangement.[1] Molecular oxo- and hydroxo-bridged iron(III) compounds are promising materials in the field of bioinorganic chemistry owing to their relevance to models of the protein active sites[2] and their activity in important biological processes.[3] Moreover, the Fe atom is a part of heteronuclear cores at metallobiosites such as purple acid phosphatase (FeZn),[4] human calcineurin (FeZn),[5] and human protein phosphatase 1 (MnFe).[6] Another significant aspect of the polynuclear oxo-bridged iron(III) compounds is their ability to possess high-spin ground states, resulting in interesting properties such as single-molecule magnetism.[7] Evidently, the combination of two or more different metal centers within one molecule can lead not only to structural diversity and complexity of the resulting heterometallic assemblies but also to their multifunctionality. These advantages have stimulated great interest in the study of systems containing dissimilar metals and have prompted the development of synthetic pathways for the preparation of polynuclear heterometallic complexes because the rational

Received: August 17, 2011
Published: November 30, 2011

design of such species is still one of the major challenges in coordination chemistry.

As has been reported earlier, a huge number of heterometallic polynuclear complexes showing sophisticated crystal structures with various nuclearities and quite interesting magnetic properties have been prepared using a synthetic approach named *direct synthesis of coordination compounds*.[8] This strategy relies on the general spontaneous self-assembly, in which one of the metals is introduced as a powder (zerovalent state) or as an oxide. The main advantage of this approach is the generation of building blocks in situ, in one reaction vessel, thus allowing elimination of the separate steps of building-block construction. The systems most extensively investigated for the preparation of polynuclear aggregates were[9]

$$M^0{}_I - M_{II}X_2/M_{II}O - HL - Solv$$

where $M_I{}^0$ = Cu; M_{II} = Zn, Pb, Cd, Co; X = halide, NCS, OAc; HL = aminoalcohols; and Solv = DMF, DMSO, CH_3OH, CH_3CN. Using such conditions and specific metal to anion ratios, a bridging coordination mode of the hydroxyl groups of the amino alcohol ligands is forced and, consequently, different metal centers are linked only by single bridging atoms instead of bridging groups, which is of great importance for magnetic materials design.

Recently, it has been shown that a direct synthesis approach can be successfully combined with the Curtis template reaction, giving the possibility of obtaining a broad range of polymeric and ionic heterometallic complexes with open-chain Schiff base ligands.[10] For this purpose, the following systems were investigated:

$$M^0{}_I - M^0{}_{II}/M_{II}O - L/L{\cdot}2HX - NH_4X - (CH_3)_2CO/CH_2O - Solv$$

$$M^0{}_I - NH_4[Cr(NCS)_4(NH_3)_2]{\cdot}H_2O - L - (CH_3)_2CO - Solv$$

where $M_I{}^0$ = Cu, Co, Ni; M_{II} = Zn, Co, Ni, Mn; X = halide, NCS; L = amines; and Solv = DMF, DMSO, CH_3OH, CH_3CN. Schiff bases derived from the reaction of aromatic aldehydes with primary amines have been the subject of yet more extensive research because of the enormous versatility of such ligands with respect to the formation of sophisticated discrete or multidimensional expanded architectures.[11] The choice of initial reagents for the condensation determines the ligand coordination fashion and allows one to utilize the blocking or bridging function of an obtained Schiff base. In the present work, we propose to expand these synthetic approaches toward the preparation of high-nuclearity heterometallic complexes containing Schiff base ligands and to explore the open-air reaction of cobalt powder and iron(II) chloride with nonaqueous solutions of chelating polydentate ligands, formed in situ, in a basic (triethylamine) medium. Here we report details of syntheses and characterizations, as well as structural features and magnetic and spectroscopic properties of $[Co^{III}{}_2Fe^{III}{}_2(L^1)_6]{\cdot}4DMF$ (**1**) and $[Co^{III}{}_4Fe^{III}{}_4(HL^2)_8(DMSO)_2]{\cdot}18DMSO$ (**2**), obtained in such a way.

EXPERIMENTAL SECTION

All chemicals were of reagent grade and were used as received. All experiments were carried out in air. Elemental analyses were performed with a FlashEa 1112 series CHNOS analyzer (for C, H, and N). Quantitative determinations of the metals were performed by atomic absorption spectroscopy.

Synthesis of $[Co^{III}{}_2Fe^{III}{}_2(L^1)_6]{\cdot}4DMF$ (1). 2-Aminobenzyl alcohol (0.62 g, 5 mmol), 5-bromosalicylaldehyde (1.01 g, 5 mmol), and triethylamine (0.7 mL, 5 mmol) were dissolved in *N*,*N*-dimethylformamide (DMF; 25 mL) in this order, forming a yellow solution, which was magnetically stirred at 50−60 °C (10 min). Then, cobalt powder (0.15 g, 2.5 mmol) and $FeCl_2{\cdot}4H_2O$ (0.25 g, 1.25 mmol) were added to the hot yellow solution of the ligand and stirred magnetically until the total dissolution of cobalt was observed (3 h). Dark-red crystals suitable for X-ray analysis were formed from the dark-red solution after 1 day. Yield: 0.54 g, 37% (per iron). Anal. Calcd for $C_{96}H_{88}Br_6Co_2Fe_2N_{10}O_{16}$: C, 49.13; H, 3.78; N, 5.97; Co, 5.02; Fe, 4.76. Found: C, 49.1; H, 3.5; N, 5.6; Co, 4.9; Fe, 4.6. IR (KBr, cm^{-1}): 3440br, 3066w, 2923w, 2846w, 1674s, 1613vs, 1594s, 1517s, 1485w, 1454s, 1413m, 1384w, 1366m, 1307m, 1167s, 1132w, 1105w, 1089w, 1074w, 1054w, 1029m, 957w, 936w, 924w, 902w, 875w, 866w, 825m, 789w, 758m, 737w, 681w, 660w, 642w, 631w, 589w, 567w, 548w, 524w, 502w, 481w, 465w, 454w, 437w, 414w. The compound is sparingly soluble in DMF and DMSO and insoluble in water.

Synthesis of $[Co^{III}{}_4Fe^{III}{}_4(HL^2)_8(DMSO)_2]{\cdot}18DMSO$ (2). This complex was prepared in a way similar to that of **1** but in a DMSO solution and using tris(hydroxymethyl)aminomethane (0.61 g, 5 mmol) with 5-nitrosalicylaldehyde (0.83 g, 5 mmol). Dark-red crystals suitable for X-ray crystallographic study were formed after 1 week after the addition of diethyl ether into the resulting dark-red solution. The crystals are not stable in air and should be kept in a mother solution. Yield: 0.23 g, 18% (per iron). Anal. Calcd for $C_{128}H_{208}Co_4Fe_4N_{16}O_{68}S_{20}$: C, 39.96; H, 5.04; N, 5.39; Co, 5.67; Fe, 5.37. Found: C, 39.6; H, 5.1; N, 5.3; Co, 5.5; Fe, 5.4. IR (KBr, cm^{-1}): 3365br, 2916w, 2865w, 1637m, 1597vs, 1546m, 1479m, 1441w, 1385w, 1311vs, 1252m, 1201w, 1141w, 1100m, 1015m, 948m, 923w, 838w, 796w, 754w, 729w, 687w, 661w, 594w, 543w, 493w, 443w. The compound is sparingly soluble in DMF and DMSO and insoluble in water.

Physical Measurements. IR spectra (4000−400 cm^{-1}) were recorded on a Perkin Elmer BX-FTIR instrument in KBr pellets.

The magnetic data were taken with a SQUID apparatus (MPMS-XL7, Quantum Design) using the RSO mode of detection. The susceptibility taken at B = 0.1 T has been corrected for the underlying diamagnetism and converted to the effective magnetic moment. The magnetization has been measured at two temperatures: T = 2.0 and T = 4.6 K.

High-frequency electron paramagnetic resonance (EPR) spectra were recorded with a home-built spectrometer at the EMR facility of NHMFL.[12] The instrument is a transmission-type device in which waves are propagated in cylindrical lightpipes. The microwaves were generated by a phase-locked oscillator (Virginia Diodes) operating at a frequency of 13 ± 1 GHz and generating its harmonics, of which the 4th, 8th, 16th, 24th, and 32nd were available. A superconducting magnet (Oxford Instruments) capable of reaching a field of 17 T was employed.

Mössbauer spectra were collected in constant acceleration mode using a spectrometer manufactured by SEE Co. Inc. (Edina, MN), which was equipped with a $^{57}Co/Rh$ γ source purchased from Cyclotron Instruments (Mainz, Germany). A Janis (Wilmington, MA) cryostat was employed for low-temperature measurements.

Crystallography. Diffraction experiments were performed on a Bruker SMART APEX-II CCD area-detector diffractometer (ω and φ rotation scans with narrow frames) equipped with graphite-monochromated Mo Kα radiation (λ = 0.710 73 Å). The data were corrected for Lorentz and polarization effects as well as for the effects of absorption (multiscan method using *SADABS*[13a]). The structures

dx.doi.org/10.1021/ic2017962 | *Inorg. Chem.* 2012, 51, 386−396

were solved by direct methods and refined by full-matrix least-squares methods on F^2 in anisotropic approximation for all non-H atoms using the *SHELXTL* program package.[13b] The positions of all H atoms in the structures were calculated regarding hybridization of the parent atom and refined using the riding model with $U_{iso}(H) = 1.5U_{iso}(C)$ for CH_3 and $U_{iso}(H) = 1.2U_{iso}(C)$ for all other parent C atoms. Details of the data collection and processing, structure solution, and refinement are summarized in Table 1.

Table 1. Crystal Data and Structure Refinement for 1 and 2.

	complex **1**	complex **2**
empirical formula	$C_{96}H_{88}Br_6Co_2Fe_2N_{10}O_{16}$	$C_{128}H_{208}Co_4Fe_4N_{16}O_{68}S_{20}$
fw	2346.78	4159.42
cryst syst	triclinic	triclinic
space group	$P\bar{1}$	$P\bar{1}$
a/Å	11.1610(7)	16.2029(5)
b/Å	14.8168(10)	16.9908(5)
c/Å	15.9280(11)	18.0633(5)
α/deg	95.336(5)	113.302(2)
β/deg	101.305(5)	100.481(2)
γ/deg	110.023(5)	90.571(2)
V/Å^3	2389.9(3)	4472.49(20)
Z	1	1
T/K	173(2)	173(2)
μ/mm^{-1}	3.217	1.522
R_{int}	0.1672	0.0827
measd/indep/obsd reflns	26 954/8397/2947	80 871/22 545/10 246
data used		
R1[$I > 2\sigma(I)$]	0.0869	0.0918
wR	0.1936	0.2503
GOF	0.885	1.041

Crystallographic data for the structures reported can be obtained free of charge via http://www.ccdc.cam.ac.uk or from the Cambridge Crystallographic Data Centre, 12 Union Road, Cambridge CB2 1EZ, U.K. [fax (+44) 1223-336-033; e-mail deposit@ccdc.cam.ac.uk] on quoting the deposition numbers CCDC 831169 (**1**) and 830304 (**2**).

RESULTS AND DISCUSSION

Synthesis and Spectroscopic Characterization. Complexes were obtained from the reaction of cobalt powder and iron chloride with a DMF (**1**) or DMSO (**2**) solution of chelating polydentate ligand, formed in situ, in a basic (triethylamine) medium, using a molar ratio of Co:$FeCl_2\cdot 4H_2O$:L = 2:1:4. The reaction was initiated and brought to completion by heating and stirring in open air. The Schiff base ligands H_2L^1 and H_4L^2 were obtained by condensation of an aldehyde [5-bromosalicylaldehyde (**1**) and 5-nitrosalicylaldehyde (**2**)] and a primary amine [2-aminobenzyl alcohol (**1**) and tris(hydroxymethyl)aminomethane (**2**)] (Scheme 1). Dark-red solutions were obtained at the end of both reactions. The microcrystals of the products were formed after standing at room temperature within 1 day (**1**) or after the addition of diethyl ether to the resulting solution over 1 week (**2**). Notably, compound **1** could also be obtained using $FeBr_2$, $Fe(NCS)_2$, or $FeCl_3$ as a starting reagent instead of $FeCl_2$, so the type of initial iron salt (neither the oxidation state of the iron or the nature of the anion) does not affect the complex composition. However, in such cases, the yield of the product was very scant compared to the $FeCl_2$ system. Both complexes can be easily synthesized over a broad range of Co:$FeCl_2\cdot 4H_2O$:L molar ratios, including an excess of the ligand or one of the metals in the system. However, the molar ratio 2:1:4, selected for preparative synthesis, not only affords higher yields but also facilitates crystallization of the final products in both cases.

Scheme 1

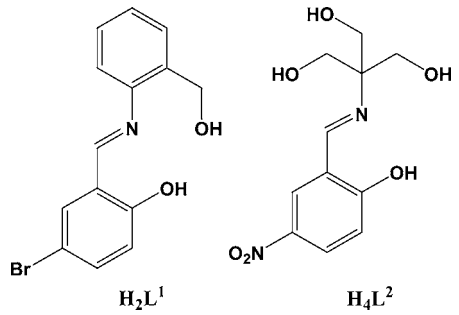

The IR spectra of complexes **1** and **2** confirmed the presence of Schiff base ligands. In the high-frequency region, broad medium-intensity bands in the 3370−3440 cm^{-1} range were attributed to ν(O−H) vibrations for both H_2L^1 and H_4L^2. Very strong bands appearing at 1613 cm^{-1} (**1**) and 1597 cm^{-1} (**2**) were assigned to ν(C=N) stretching vibrations. Also, a very strong $\nu(NO_2)$ absorption at 1311 cm^{-1} was observed in the spectrum of **2**. The presence of the solvate molecules in the compounds can be identified by the strong peak at 1674 cm^{-1} (for DMF, **1**) and medium-intensity bands at 1015 and 948 cm^{-1} (for DMSO, **2**).

Crystal Structures. The molecular structure of **1** is based on the tetranuclear core $\{Co^{III}_2Fe^{III}_2(\mu\text{-}O)_6\}$ with the nonlinear Co1···Fe1···Fe1′···Co1′ chain arrangement, where all metal pairs are joined by two O bridges from the deprotonated Schiff base ligands (Figure 1). The structure is

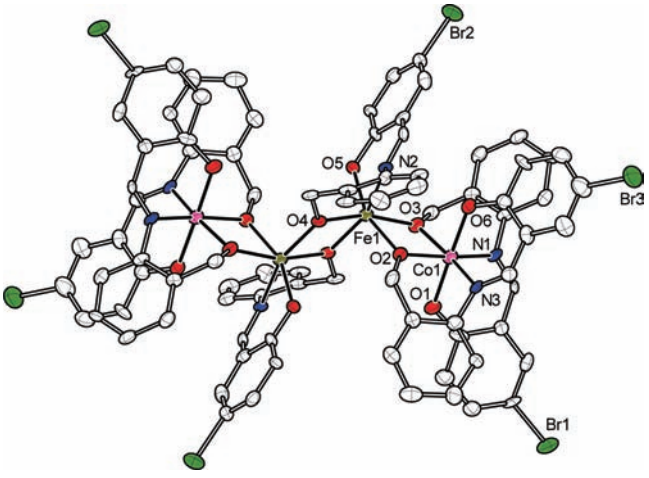

Figure 1. Molecular structure of **1** with atom numbering. The H atoms are omitted for clarity, and the non-H atoms are shown as 30% ellipsoids.

centrosymmetric with the inversion center located at the midpoint of the Fe_2O_2 unit and with all of the metal atoms lying in one plane (Figure 2). The consecutive $M_4(\mu\text{-}X)_6$ molecular structural type observed in **1** is quite common and was widely described for many tetranuclear aggregates (ca. 300 hits according to CSD[14]), but the present complex is rather a rare example of a heterometallic iron-containing compound of such type (5 hits[15] in CSD) and only five

dx.doi.org/10.1021/ic2017962 | *Inorg. Chem.* 2012, 51, 386−396

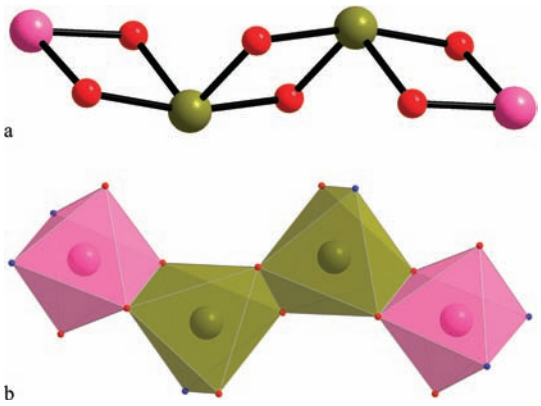

Figure 2. Ball-and-stick (a) and polyhedral (b) representations of the tetranuclear $\{Co_2Fe_2(\mu\text{-}O)_6\}$ core in **1**. Color scheme: Co, pink; Fe, olive; O, red; N, blue.

complexes with Fe^{III} based on the $M_4(\mu\text{-}O)_6$ core were found.[15a,16]

Both coordination environments of Co^{III} and Fe^{III} are formed by donor atoms of Schiff base ligands, which act in a tridentate (N,O,O) fashion. The Co^{III} atom displays an almost regular octahedral coordination geometry comprised of four O and two N atoms of two chelating tridentate ligands. The Co−O(N) distances vary from 1.896(8) to 1.925(9) Å, while the *cis* bond angles around the Co range from 78.1(3)° to 99.2(4)° and the *trans* bond angles span from 169.0(3)° to 178.1(3)° (Table 2).

Table 2. Selected Geometrical Parameters (Distances/Å and Angles/deg) for 1[a]

Co1−O1	1.896(8)	Fe1−O2	1.981(7)
Co1−O2	1.899(7)	Fe1−O3	1.997(7)
Co1−O3	1.899(7)	Fe1−O4	2.000(7)
Co1−O6	1.906(8)	Fe1−O4[a]	1.961(7)
Co1−N1	1.924(9)	Fe1−O5	1.972(7)
Co1−N3	1.925(9)	Fe1−N2	2.140(9)
Co1···Fe1	3.054(7)	Fe1···Fe1[a]	3.168(14)
O1−Co1−O3	92.5(3)	O2−Fe1−O3	73.9(3)
O1−Co1−O2	90.0(3)	O2−Fe1−O4	92.1(3)
O1−Co1−O6	178.1(3)	O2−Fe1−O4[a]	100.3(3)
O2−Co1−O6	91.8(3)	O3−Fe1−O4	163.8(3)
O3−Co1−O2	78.1(3)	O3−Fe1−O4[a]	100.1(3)
O3−Co1−O6	87.0(3)	O4−Fe1−O4[a]	73.8(4)
O1−Co1−N1	88.8(4)	O5−Fe1−O2	158.4(3)
O1−Co1−N3	90.3(4)	O5−Fe1−O3	88.6(3)
O2−Co1−N1	169.4(3)	O5−Fe1−O4	106.7(3)
O2−Co1−N3	91.3(3)	O2−Fe1−N2	87.9(3)
O3−Co1−N1	91.5(3)	O3−Fe1−N2	103.0(3)
O3−Co1−N3	169.0(3)	O4−Fe1−N2	84.4(3)
O6−Co1−N1	89.4(4)	O4[a]−Fe1−N2	156.8(3)
O6−Co1−N3	90.5(4)	O5−Fe1−N2	83.6(3)
N1−Co1−N3	99.2(4)	O5−Fe1−O4[a]	95.1(3)

[a]Symmetry transformations used to generate equivalent atoms: a, $-x + 1, -y, -z$.

The geometry around the Fe^{III} atom also reveals a distorted octahedral environment but with a NO_5 donor set [Fe−O(N) bond lengths vary in the range 1.961(7)−2.140(9) Å; the *cis* and *trans* O−Fe−O(N) bond angles range from 73.8(4)° to 106.7(3)° and from 156.8(3)° to 163.8(3)°, respectively].

Although the prediction of the composition and crystal structure of coordination compounds represents quite a complicated task, some aspects concerning the complex formation can be understood by comparing the structures of **1** with the previously reported heterotrimetallic complex $[FeCuCo(Dea)_3(NCS)_2(MeOH)]_2\cdot 3.2H_2O$ (H_2Dea = diethanolamine).[17] As can be seen in Figures 2a and 3, both

Figure 3. Ball-and-stick representation of the hexanuclear $\{Cu_2Co_2Fe_2(\mu\text{-}O)_{10}\}$ core in $[FeCuCo(Dea)_3(NCS)_2(MeOH)]_2\cdot 3.2H_2O$ (H_2Dea = diethanolamine).[17] Color scheme: Cu, cyan; Co, pink; Fe, olive; O, red.

structures contain a centrosymmetric $\{Co_2Fe_2(\mu\text{-}O)_6\}$ fragment with the same metal arrangements. In the heterotrimetallic complex, the Co atom coordinates two diethanolamine ligands, forming a typical *cis,fac*-$[Co^{III}(Dea)_2]^-$ block that connects neighboring copper and iron polyhedra. The Co^{III} atom in **1** is part of a very similar unit, *cis,fac*-$[Co^{III}(L^1)_2]^-$, which is, however, formed by a ligand more bulky than diethanolamine. As a result, the *cis,fac*-$[Co^{III}(L^1)_2]^-$ block joins only one adjacent Fe^{III} atom involving only two O atoms, in contrast to the *cis,fac*-$[Co^{III}(Dea)_2]^-$ block in which all four O atoms coordinate to other metal centers. Thus, in the case of **1**, the *cis,fac*-$[Co^{III}(L^1)_2]^-$ unit plays the role of a terminal block without the geometrical possibility of arranging this tetrametallic fragment into a polymeric chain. Taking into account the facial coordination mode of the ligand, one can predict the intermetallic Co−Fe−Fe′ angle to be close to 120°, which represents the theoretical value for the combination of three regular octahedra fused via common edges. The actual angle of 125.7° is in conformity with this expected value and with that observed earlier for a comparable heterotrimetallic Cu/Co/Fe structure (101.9°).

The molecular complex **2** has an octanuclear core $\{Co^{III}_4Fe^{III}_4(\mu\text{-}O)_{14}\}$ and could be described as a combination of two $\{CoFe(HL^2)_2\}$ and two $\{CoFe(HL^2)_2(DMSO)\}$ moieties successively joined by bridging O atoms from the Schiff base ligands (Figure 4). The structure is also centrosymmetric, with the inversion center located at the midpoint of the Fe_2O_2 fragment, similar to **1**. All Schiff base ligands in the structure are triply deprotonated and act in a tetradentate (N,O,O,O) fashion, leaving one OH group uncoordinated. In both **1** and **2**, the ligands have two principal functions, the molecular-structure-type predetermination and metal-ion charge compensation, so that the complexes do not require counterions.

Compound **2** contains two crystallographycally independent Co^{III} atoms, Co1 and Co2, and two independent Fe^{III} atoms, Fe1 and Fe2, each of them having a distorted octahedral environment with N_2O_4 and O_6 donor sets for Co and Fe, respectively. The coordination spheres of Co1, Co2, and Fe1 involve only the Schiff base ligands, while the coordination sites around Fe2 are occupied by O atoms from Schiff base ligands and from a DMSO molecule. The Co−O(N) bond lengths range from 1.883(6) to 1.912(5) Å, while the Fe−O distances vary from 1.870(5) to 2.080(5) Å (Table 3). The O(N)−M−$O(N)_{trans}$ angles vary from 174.0(2) to 177.90(19)° for Co^{III}

dx.doi.org/10.1021/ic2017962 | Inorg. Chem. 2012, 51, 386−396

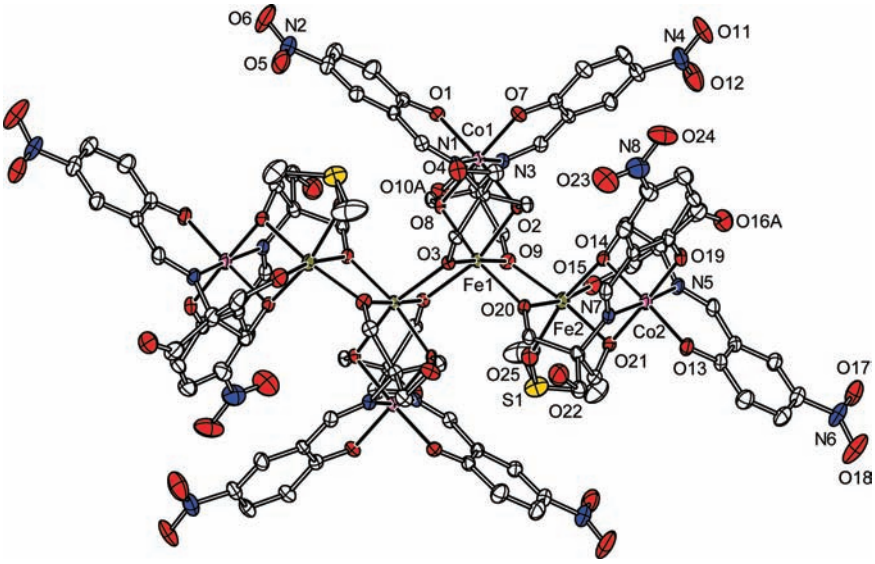

Figure 4. Molecular structure of **2**, showing the atom numbering, with 30% probability displacement ellipsoids. H atoms are omitted for clarity.

and from 161.69(17) to 176.86(18)° for Fe^{III}. The search via CSD revealed two main configurations of highly nuclear, namely, octanuclear, complexes: single-stranded wheels and closed, cagelike clusters.[1a,18] Complex **2** does not belong to any of these common polynuclear families and shows an absolutely different and quite rare manner of metal arrangement (Figure 5). According to CSD, a structure similar to that of **2** has been reported only for a homometallic nickel(II) complex, $Ni_8(L)_4Cl_8\cdot(H_2O)_{0.5}$, where L = Schiff base, *N,N′-o*-phenylenebis(salicylideneimine).[19] Formation of the unusual structure of **2** can be understood if one considers the scheme presented in Figure 6. The coordination mode of the Schiff base ligands to the Co center in **2** leads to the formation of a *trans,mer*-$[Co^{III}(HL^2)_2]^{3-}$ unit with a quite typical for Co^{III} N_2O_4 octahedral environment. The participation of Fe^{III} in such a reaction is less probable. This is evidenced by the statistics from the CSD: the abundance of MN_2O_4 complexes is much greater for cobalt than for iron (9.6 and 2.0%, respectively, among all cobalt or iron structures). At the next stage, free iron ion is coordinated to form a binuclear $\{CoFe(HL^2)_2\}$ block (*a*), where the free sites in the coordination environment of iron are occupied by solvent molecules. The reaction of two blocks *a* leads to a tetranuclear fragment *b*. In this way, fragment *a* can be considered as a secondary building block, which could pack into the polymeric chain involving Fe−(μ-O)−Fe′ linkages. However, the steric hindrance of bulky nitrobenzene rings prevents the coupling of more than two binuclear $\{CoFe(HL^2)_2\}$ blocks *a* (Figure 6), lying in one plane, and the coordination of a third block *a* can only occur with its ca. 90° turn, making it a terminal ligand. One can suppose that in the absence of steric problems the 1D heterometallic coordination polymer could be formed.

Finally, when the crystal structures of **1** and **2** are analyzed, it can be concluded that both *cis,fac*-$[Co^{III}(L^1)_2]^-$ and *trans,mer*-$[Co^{III}(HL^2)_2]^{3-}$ moieties seem to have a predominant and crucial function in the formation of the heterometallic complex because precisely these fragments define the molecular structural type and nuclearity of the final polymetallic assembly.

Magnetic Properties. Thermal variation of the effective magnetic moment in complex **1** is displayed in Figure 7. At room temperature, μ_{eff} equals 6.8 μ_B, and upon cooling, it decreases gradually to μ_{eff} = 2.2 μ_B at T = 10 K. Below 10 K, it shows a plateau, and then it drops down to μ_{eff} = 2.0 μ_B at T = 1.9 K. This behavior is a fingerprint of the dominating antiferromagnetic interaction. However, the maximum of the susceptibility, expected at $T_{max} = |J/k|/0.347$ is not seen because it is overlapped by a strong signal of the paramagnetic impurity (Figure 8). The limiting value of the effective magnetic moment for two noninteracting high-spin Fe^{III} centers equals $\mu_{eff} = [2g_{Fe}^2 S_{Fe}(S_{Fe} + 1)]^{1/2}\mu_B$, which amounts to 8.37 μ_B when g_{Fe} = 2.0. The molar magnetization per formula unit has a saturation limit $M_1 = M_{mol}/N_A\mu_B = 2g_{Fe}S_{Fe}$, which yields M_1 = 10 for $S_{Fe} = {}^5/_2$.

The magnetic data were fitted by using the spin Hamiltonian

$$\hat{H}_{dim} = -J(\vec{S}_1\cdot\vec{S}_2)\hbar^{-2} + \mu_B g\vec{B}(\vec{S}_1 + \vec{S}_2)\hbar^{-1} + D(\hat{S}_{1z}^2 - \hat{S}_1^2/3)\hbar^{-2} + D(\hat{S}_{2z}^2 - \hat{S}_2^2/3)\hbar^{-2} \quad (1)$$

The susceptibility data were further corrected for the presence of the paramagnetic impurity that obeys the Curie−Weiss law

$$\chi'_{mol} = (1 - x_{PI})\chi_{dim} + 2x_{PI}(N_A\mu_0\mu_B^2/k)g_{PI}^2 \times S_{PI}(S_{PI} + 1)/[3(T - \Theta)] + \alpha \quad (2)$$

($S_{PI} = {}^5/_2$). The constant term α compensates the signal of the sample holder, uncertainties of the correction for the underlying diamagnetism of the sample, and the temperature-independent paramagnetism. The magnetization data were corrected by the Brillouin-function behavior for the paramagnetic impurity

$$M'_{mol} = (1 - x_{PI})M_{dim} + 2x_{PI}(N_A\mu_B g_{PI}S_{PI}) \times B_{S=5/2}(g_{PI}\mu_B B/kT) \quad (3)$$

dx.doi.org/10.1021/ic2017962 | *Inorg. Chem.* 2012, 51, 386−396

Table 3. Selected Geometrical Parameters (Distances/Å and Angles/deg) for 2[a]

Co1−O1	1.894(4)	Fe1−O2	2.051(4)
Co1−O2	1.896(4)	Fe1−O3	1.990(4)
Co1−O7	1.887(4)	Fe1−O3[a]	2.021(4)
Co1−O8	1.894(4)	Fe1−O8	2.033(4)
Co1−N1	1.912(5)	Fe1−O9	1.979(4)
Co1−N3	1.909(5)	Fe1−O20	1.973(4)
Co2−O13	1.893(5)	Fe2−O9	2.023(4)
Co2−O14	1.898(4)	Fe2−O14	2.045(5)
Co2−O19	1.886(5)	Fe2−O15	1.870(5)
Co2−O21	1.903(5)	Fe2−O20	2.038(4)
Co2−N5	1.883(6)	Fe2−O21	2.030(5)
Co2−N7	1.902(5)	Fe2−O25	2.080(5)
Co1···Fe1	3.00	Fe1···Fe1[a]	3.14
Co2···Fe2	2.98	Fe1···Fe2	3.14
O1−Co1−O2	176.10(18)	O2−Fe1−O3	90.68(16)
O1−Co1−O7	90.4(2)	O2−Fe1−O3[a]	161.69(17)
O1−Co1−O8	91.69(18)	O2−Fe1−O8	77.16(18)
O2−Co1−O7	93.52(19)	O2−Fe1−O9	90.51(17)
O2−Co1−O8	84.42(17)	O2−Fe1−O20	96.25(17)
O7−Co1−O8	177.90(19)	O3−Fe1−O3[a]	76.82(18)
O1−Co1−N1	96.1(2)	O3−Fe1−O8	92.33(17)
O1−Co1−N3	88.9(2)	O3−Fe1−O9	176.86(18)
O2−Co1−N1	83.8(2)	O3−Fe1−O20	99.72(17)
O2−Co1−N3	91.0(2)	O8−Fe1−O3[a]	89.87(16)
O7−Co1−N1	87.7(2)	O8−Fe1−O9	90.77(17)
O7−Co1−N3	95.5(2)	O8−Fe1−O20	166.38(17)
O8−Co1−N1	92.45(19)	O9−Fe1−O3[a]	102.68(18)
O8−Co1−N3	84.1(2)	O9−Fe1−O20	77.25(18)
N1−Co1−N3	174.0(2)	O20−Fe1−O3[a]	98.99(17)
O13−Co2−O14	177.4(2)	O9−Fe2−O14	101.07(18)
O13−Co2−O19	90.7(2)	O9−Fe2−O15	95.9(2)
O13−Co2−O21	92.4(2)	O9−Fe2−O20	74.82(17)
O14−Co2−O19	91.7(2)	O9−Fe2−O21	165.62(18)
O14−Co2−O21	85.2(2)	O9−Fe2−O25	92.02(19)
O19−Co2−O21	176.8(2)	O14−Fe2−O15	91.2(2)
O13−Co2−N5	96.5(2)	O14−Fe2−O20	86.79(18)
O13−Co2−N7	88.3(2)	O14−Fe2−O21	78.27(18)
O14−Co2−N5	84.7(2)	O14−Fe2−O25	164.7(2)
O14−Co2−N7	90.4(2)	O15−Fe2−O20	169.9(2)
O19−Co2−N5	86.7(3)	O15−Fe2−O21	98.4(2)
O19−Co2−N7	96.2(2)	O15−Fe2−O25	95.3(2)
O21−Co2−N5	92.1(2)	O20−Fe2−O25	89.11(19)
O21−Co2−N7	84.8(2)	O21−Fe2−O20	90.82(17)
N5−Co2−N7	174.4(2)	O21−Fe2−O25	87.1(2)

[a]Symmetry transformations used to generate equivalent atoms: a, $2 - x$, $2 - y$, $1 - z$.

The fitting procedure has been applied simultaneously to the susceptibility and magnetization data sets by minimizing the error functional[20]

$$F = \left[\sum_{i}^{N} |\chi_i^c - \chi_i^o|/\chi_i^o\right]\left[\sum_{j}^{M} |M_j^c - M_j^o|/M_j^o\right] \rightarrow \min \quad (4)$$

During the optimization, it was found that the J, g, and α values are mutually correlated, so that several solutions of the same quality exist. Because J is about -30 cm^{-1}, M_{dim} is negligible at low temperature; consequently, the D value is not reflected in the magnetization data, and thus it cannot be bracketed reliably. The magnetization data serve for determination of the paramagnetic impurity.

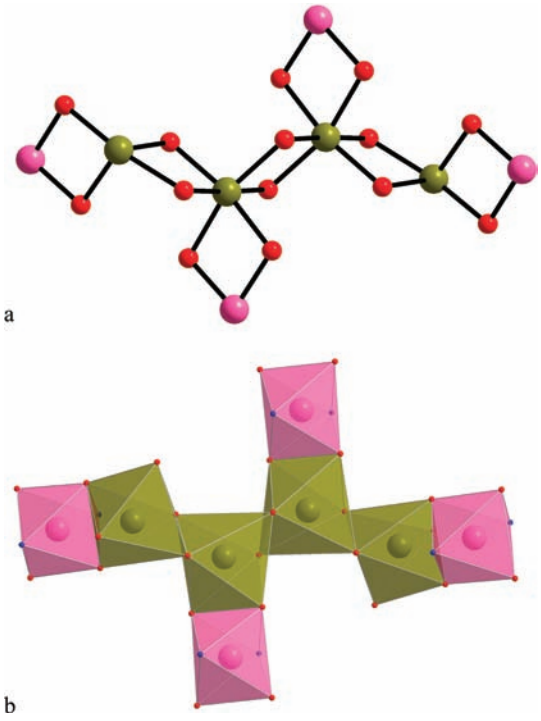

Figure 5. Ball-and-stick (a) and polyhedral (b) representations of the octanuclear $\{Co_4Fe_4(\mu\text{-}O)_{14}\}$ core in **2**. Color scheme: Co, pink; Fe, olive; O, red; N, blue.

One set of magnetic parameters has been obtained by fixing the value of $g = 2.01$ and switching off the D parameter; then $J/hc = -31.9$ cm^{-1}, $\alpha = 20 \times 10^{-9}$ m^3 mol^{-1} (SI units), $x_{PI} = 0.056$, and $g_{PI} = 2.07$ [$R(\chi) = 0.051$ and $R(M) = 0.044$]. The negative value of the Fe−Fe exchange coupling constant matches the large angle Fe−O−Fe of the superexchange path. The fits of the magnetization contribution due to the paramagnetic impurity with the Brillouin function are very good, which proves that D(PI) is negligible. Note that the content of PI can vary from one sample batch to another, and it can depend on the sample history (crystallinity, defects, grinding, etc.).

The magnetic behavior of complex **2** is interpreted according to the model of a finite chain of four $S_{Fe} = {}^5/_2$ centers. The limiting value of the effective magnetic moment for four noninteracting high-spin Fe^{III} centers is $\mu_{eff} = [4g^2S_{Fe}(S_{Fe} + 1)]^{1/2}\mu_B$, which amounts to 11.8 μ_B when all $g = 2.0$. Upon cooling from room temperature, the effective magnetic moment gradually decreases from $\mu_{eff} = 9.5\ \mu_B$ to $1.8\ \mu_B$ at $T = 2.0$ K (Figure 9). This feature confirms the dominating antiferromagnetic coupling between the magnetic centers. The molar magnetic susceptibility increases with a decrease in the temperature to 2.0 K, showing no maximum.

The saturation limit of the molar magnetization per formula unit equals $M_1 = 4gS_{Fe}$, which yields $M_1 = 20$ for $S_{Fe} = {}^5/_2$. The measured magnetization adopts a value of only $M_1 = 0.96$ at

dx.doi.org/10.1021/ic2017962 | Inorg. Chem. 2012, 51, 386−396

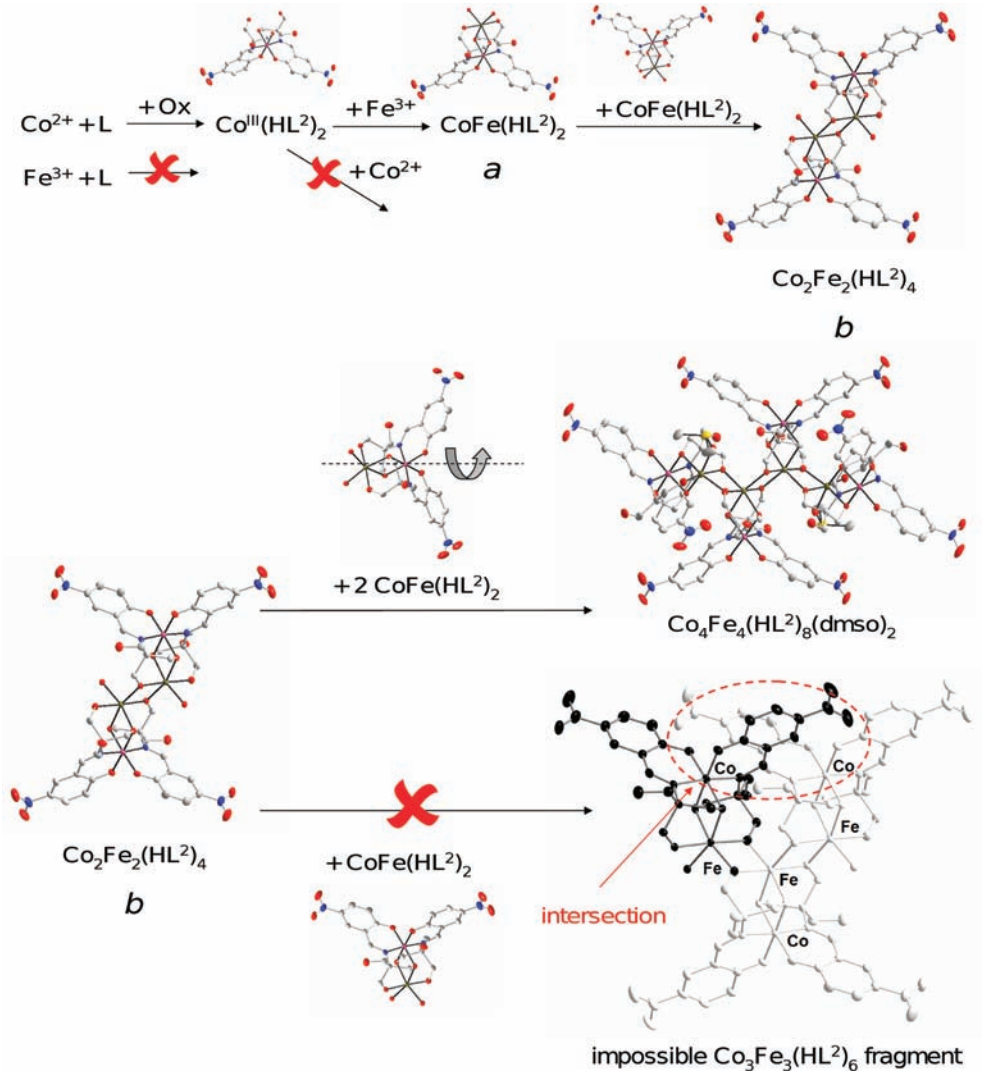

Figure 6. Proposed pathway for the formation of **2**.

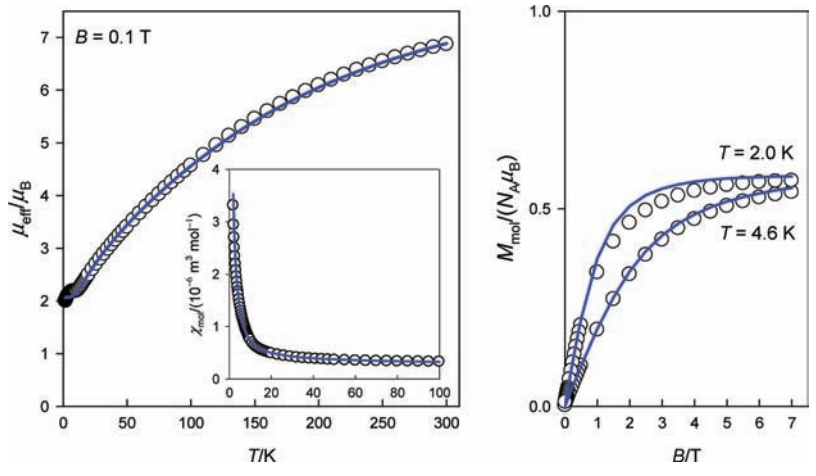

Figure 7. Magnetic functions for **1**: (left) temperature dependence of the effective magnetic moment; (right) field dependence of the magnetization. Inset: temperature dependence of the molar magnetic susceptibility. Open circles: experimental data. Lines: fitted data.

T = 4.6 K. This reduction is a fingerprint of a dominating antiferromagnetic exchange, eventually combined with single-ion anisotropy. The Fe^{III} centers could be considered as isotropic ($g \sim 2.0$; $D \sim 0$).

dx.doi.org/10.1021/ic2017962 | *Inorg. Chem.* 2012, 51, 386–396

The magnetic data were reproduced using a spin Hamiltonian

$$\hat{H} = -J(\vec{S}_1\cdot\vec{S}_2 + \vec{S}_2\cdot\vec{S}_3 + \vec{S}_3\cdot\vec{S}_4)\hbar^{-2} + \mu_B Bg(\hat{S}_{1z} + \hat{S}_{2z} + \hat{S}_{3z} + \hat{S}_{4z})\hbar^{-1} \quad (5)$$

The additional correction accounts for the presence of a paramagnetic impurity

$$\chi'_{mol} = (1 - x_{PI})\frac{\chi_{mol}}{1 - (zj/N_A\mu_0\mu_B{}^2)\chi_{mol}} + 4x_{PI}(N_A\mu_0\mu_B{}^2/k)g_{PI}{}^2S_{PI}(S_{PI} + 1)/3T + \alpha \quad (6)$$

for which fulfillment of the Curie law is expected ($S_{PI} = {}^5/_2$; $g_{PI} = 2.0$). The eventual molecular-field correction zj accounts for the nearest-neighbor interaction. The magnetization has been corrected by adding a Brillouin function for the paramagnetic impurity:

$$M'_{mol} = (1 - x_{PI})M_{mol} + 4x_{PI}(N_A\mu_B g_{PI}S_{PI}) \times B_{S=5/2}(g_{PI}\mu_B B/kT) \quad (7)$$

The factor 4 reflects the fact that one tetranuclear unit produces four mononuclear fragments.

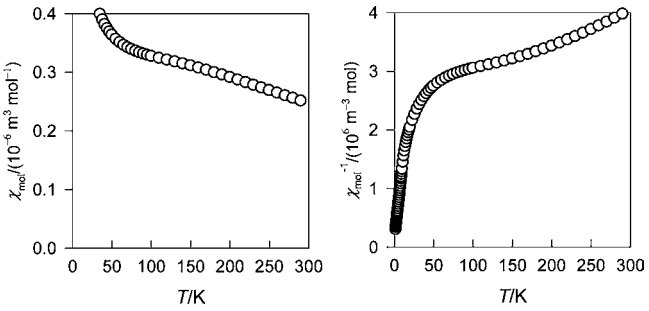

Figure 8. Temperature dependence of the molar magnetic susceptibility (left) and its inverse (right) for **1**.

The fitting procedure has been applied simultaneously for two data sets: the temperature dependence of the susceptibility and the field dependence of the magnetization. It converged to the following set of magnetic parameters: $J/hc = -20.1$ cm^{-1}, $g = 2.0$ (fixed), $\alpha = 1.5 \times 10^{-9}$ m^3 mol^{-1}, $x_{PI} = 0.024$, and $zj/hc = -0.12$ cm^{-1} [$R(\chi) = 0.016$; $R(M) = 0.032$].

A highly negative value of J is typical for the Fe^{III} centers linked by O-donor ligands. Gorun and Lippard correlated the exchange coupling constant versus the shortest Fe−O contact (P) along a superexchange path Fe−O−Fe in a series of dinuclear iron(III) complexes.[23] The data are grouped into two clusters: one for a very short P (~1.80 Å), where $J \sim -100$ cm^{-1}, and one for "normal" range P (~1.96−2.00 Å), where J is about −20 cm^{-1}. Our data span the second range: P = 1.961 Å with $J = -32$ cm^{-1} for **1** and P = 1.973 Å with $J = -20$ cm^{-1} for **2**.

High-Field and High-Frequency EPR Spectroscopy. Complex **1** exhibited at higher temperatures poorly resolved high-frequency EPR spectra with most of the intensity concentrated in a broad line around $g = 2$. A "half-field" transition, which typically occurs in triplet states, was also seen. The resolution improved considerably at temperatures lower than 100 K, allowing identification of transitions occurring within the $S = 1$ and 2 states of the diiron system (Figure 10). At these lower temperatures, the EPR spectra reveal a doubling of the "half-field" line, which was not seen at higher temperatures. The complex may thus undergo a phase transition in which two rather similar dinuclear units are formed. Signals due to monomeric impurities were also seen. Because the exchange integral in this complex is sizable, the coupled-spin states are well separated and spectra of the $S = 1$, 2, etc., states can be analyzed separately by using the spin Hamiltonian

$$\hat{H}_S = \mu_B B\cdot g\cdot\hat{S} + D\{\hat{S}_z{}^2 - S(S + 1)/3\} + E(\hat{S}_x{}^2 - \hat{S}_y{}^2) \quad (8)$$

in which the zero-field-splitting parameters are different in each coupled-spin state S. In the triplet state, we found $g_x = 2.002$, $g_y = 2.012$, $g_z = 2.012$, $D/hc = -2.01$ cm^{-1}, and $E/hc = -0.50$ cm^{-1}.

The parameters for the quintet state ($S = 2$) were $g_x = 2.006$, $g_y = 2.015$, $g_z = 2.008$, $D/hc = -0.338$ cm^{-1}, and $E/hc = -0.112$ cm^{-1}. The tiny g anisotropy could be detected only

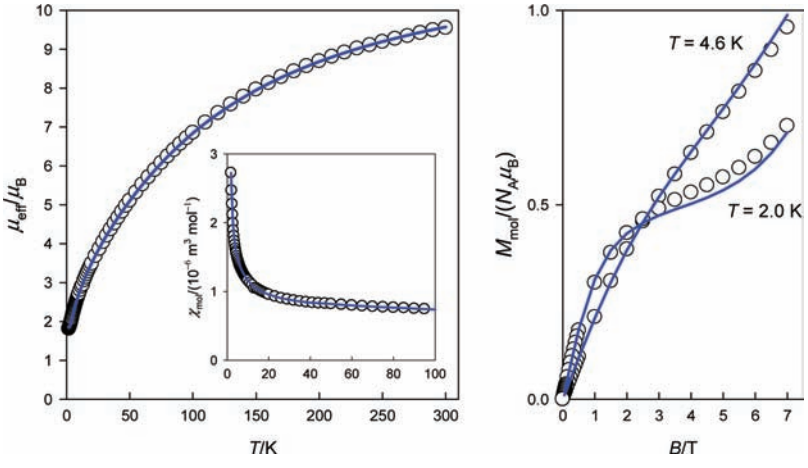

Figure 9. Magnetic functions for **2**: (left) temperature dependence of the effective magnetic moment; (right) field dependence of the magnetization per formula unit. Inset: temperature dependence of the molar magnetic susceptibility (SI units). Open circles: experimental data. Lines: fitted data.

dx.doi.org/10.1021/ic2017962 | Inorg. Chem. 2012, 51, 386−396

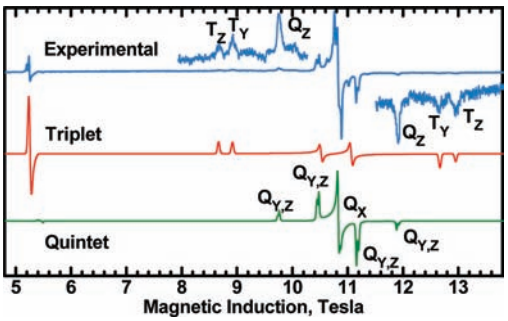

Figure 10. EPR spectra of **1**. Top: EPR spectrum recorded with 304.8 GHz at 50 K. Center: simulated triplet spectrum. Bottom: simulated quintet spectrum. Letters T and Q designate the triplet and quintet resonances, while the indices X, Y, and Z mark the molecular orientations. High rhombicity of the spin-Hamiltonian parameters (E close to $D/3$) causes the Z and Y lines to almost overlap and produces a pair of closely spaced X resonances in the triplet spectrum and only one central X resonance in the quintet spectrum.

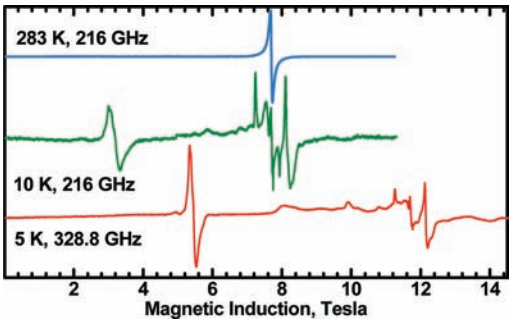

Figure 11. EPR spectra of **2**. A triplet spectrum can be recognized with g_{xyz} = 2, D/hc = −3.36 cm^{-1}, and E/hc = 0.98 cm^{-1}.

because of the very high magnetic fields used in this study. The spectra quality was barely sufficient for determination of the D parameter sign, which sometimes can be done for binuclear systems in high-field EPR.[21]

The zero-field-splitting parameters observed in various spin states contain contribution due to the anisotropic interactions between the two ions as well as a contribution related to the zero-field splitting on separate high-spin Fe^{III} ions. They can be expressed as

$$D_S = \alpha_S D_e + \beta_S D_c, \quad E_S = \alpha_S E_e + \beta_S E_c \tag{9}$$

where the index S designates a coupled-spin state (1, 2, ...), D_e and E_e are the interaction parameters, while D_c and E_c refer to each of the two Fe ions. Coefficients α_S and β_S (and formulas for them) can be found in many texts.[20a,21c,22]

For a system of two $S = {}^5/_2$ ions, $\alpha_1 = 3.7$, $\beta_1 = -6.4$, $\alpha_2 = 41/42$, $\beta_2 = -20/21$, and D_c and D_e can be evaluated. With both D_1 and D_2 being negative, D_c/hc = 0.25 cm^{-1} and D_e/hc = −0.11 cm^{-1} were obtained. The main contribution to D_e in an iron(III) dimer is expected to be the due to the magnetic dipolar interaction. The anisotropic exchange interactions, which are the main contributors to D_e in copper dimers,[21a,b,22b,c] rely on the spin−orbit coupling and should be small in the present case of two $^6A_1$ ions. The dipolar contribution to D_e is, assuming a point−dipole model[21c,22]

$$D_e^{\text{dipolar}} = -3g_z^2\mu_B^2/R^3 \tag{10}$$

where R is the interion distance and equals 3.17 Å, resulting in D_e^{dipolar}/hc = −0.16 cm^{-1}, in reasonable agreement with −0.11 cm^{-1} found above. The latter formula does not take electron delocalization into account, and the calculated dipolar interaction is likely to be overestimated.

Complex **2** exhibited at room temperature a high-field EPR spectrum consisting of only one, relatively narrow (ca. 500 G peak-to-peak distance), symmetric resonance at g = 2 (Figure 11). This must be due to extensive relaxation processes between the very many possible states in the tetranuclear iron(III) system. The exchange interactions in the system of 1296 (6^4) wave functions give rise to the coupled-spin states, with the spin numbers ranging from 0 to 10. Opposite to dimeric complexes like **1**, where each spin state with a given S number is unique, in the tetramer, there are many states of the same total spin S, like 15 states with S = 1 (Table 4), which, in general, differ in energy.

Under such circumstances, interpretation of the EPR spectra must be very limited. The single-line spectrum observed at room temperature splits at low temperatures into a much more complicated one, revealing the presence of at least one triplet spectrum with strongly rhombic zero-field splitting: D of about 3.4 cm^{-1} and E of ∼1 cm^{-1}. A quintet spectrum with D ∼ 0.15 cm^{-1} also appears to be present. As expected, there are many more resonances that cannot be clearly assigned. One should also be aware that, with a relatively weak exchange coupling, the total spin S may not be a good quantum number because the anisotropic metal−metal interactions mix various spin states and the validity of the spin Hamiltonian (8), which works with well-separated states of a total spin S, may be limited.[20a,21c,22c]

Mössbauer Spectroscopy. The Mössbauer parameters for **1**, the isomer shift IS = 0.522(2) mm s^{-1}, and the quadrupole splitting QS = 0.576(2) mm s^{-1} are consistent with high-spin Fe^{III} in the $^6A_1$ state. The Mössbauer spectrum of **2** (Figure 12, bottom) is composed of two doublets showing different quadrupole splittings. At 77 K, an IS of 0.525(1) mm s^{-1} (versus α-iron) and a QS of 1.19(2) mm s^{-1} were observed for one of the doublets, while IS = 0.503(5) mm s^{-1} and QS = 0.414(6) were found for the other doublet. The integrated Mössbauer intensity ratio was 0.52:1, with the latter doublet being more intense. It appears clear that the two doublets must be related to the "outer" two and the "inner" two Fe atoms in the four-membered chain. The Mössbauer intensity depends on the Lamb−Mössbauer factor (probability of the recoil-free γ absorption), which can be calculated from

$$f_{LM} = \exp(-4\pi^2\langle x^2\rangle/\lambda^2) \tag{11}$$

where $\langle x^2\rangle$ is the mean-squared vibrational amplitude of an Fe atom and λ = 0.86 Å is the γ-radiation wavelength. $\langle x^2\rangle$ can be taken as the isotropic temperature factor U_{iso} from X-ray structure analysis. In our case, these factors are 0.0326 and 0.0228 Å^2 (see the CIF files in the Supporting Information) for the outer and inner Fe atoms, respectively, resulting in f_{LM} factors of 0.175 and 0.300. The ratio 0.175:0.300 = 0.58:1 closely approaches the measured intensity ratio of the two doublets, thus allowing assignment of the more intense doublet with a smaller QS to the inner Fe atoms.

dx.doi.org/10.1021/ic2017962 | Inorg. Chem. 2012, 51, 386−396

Table 4. Number of States with a Total Spin S in a System of Four $S = {}^5/_2$ Ions

total spin S	10	9	8	7	6	5	4	3	2	1	0
number of states	1	3	6	10	15	21	24	24	21	15	6

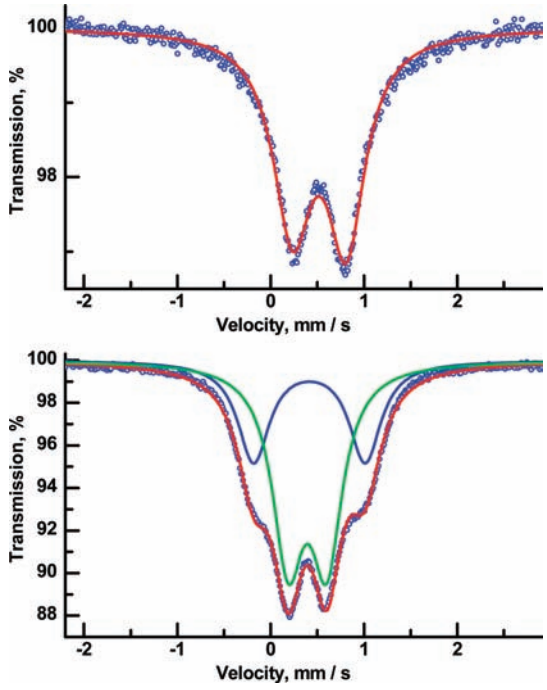

Figure 12. Mössbauer spectra of **1** (top) and **2** (bottom) collected at 77 K. Parameters for **1**: IS = 0.522(2) mm s^{-1}, QS = 0.576(2) mm s^{-1}. Parameters for **2**: doublet assigned to the inner Fe atoms, IS = 0.503(1) mm s^{-1}, QS = 0.414(6) mm s^{-1} (green); doublet assigned to the outer Fe atoms, IS = 0.525(1) mm s^{-1}, QS = 1.19(2) mm s^{-1} (blue).

CONCLUSIONS

The present work has extended the direct synthesis approach to the preparation of heterometallic complexes of high nuclearity with polydentate Schiff base ligands formed in situ. Open-air reactions of cobalt powder and iron chloride with a solution containing a condensation product of an aldehyde [5-bromosalicylaldehyde (**1**) and 5-nitrosalicylaldehyde (**2**)] and a primary amine [2-aminobenzyl alcohol (**1**) and tris(hydroxymethyl)aminomethane (**2**)] dissolved in either DMF (**1**) or DMSO (**2**) yielded two new complexes, $[Co^{III}_2Fe^{III}_2(L^1)_6]\cdot 4DMF$ (**1**) and $[Co^{III}_4Fe^{III}_4(HL^2)_8(DMSO)_2]\cdot 18DMSO$ (**2**). Although the $\{M_4(\mu\text{-}X)_6\}$ molecular structure type of **1** represents an extremely widespread topology for tetranuclear complexes, as far we are aware, our compound **1** based on the $\{Co_2Fe_2(\mu\text{-}O)_6\}$ core is the first heterometallic iron-containing complex with a chainlike metal arrangement built by O bridges only. The crystal structure of **2** represents the first example of the heterometallic octanuclear core $\{Co_4Fe_4(\mu\text{-}O)_{14}\}$ with a quite rare type of metal arrangement formed by two pairs of $\{CoFe(HL^2)_2\}$ and $\{CoFe(HL^2)_2(DMSO)\}$ moieties joined by O atoms from Schiff base ligands. Analysis of the crystal structures of **1** and **2** revealed that in both cases the Co^{III} moieties *cis,fac*-$[Co^{III}(L^1)_2]^-$ (**1**) and *trans,mer*-$[Co^{III}(HL^2)_2]^{3-}$ (**2**) have a predominant role in the definition of the molecular structural type and nuclearity of the final polymetallic assembly. The magnetic investigations reveal antiferromagnetic coupling between paramagnetic centers in both complexes.

ASSOCIATED CONTENT

Supporting Information

CIF files of crystallography data for structures **1** and **2**. This material is available free of charge via the Internet at http://pubs.acs.org.

AUTHOR INFORMATION

Corresponding Author

*E-mail: nesterova@univ.kiev.ua. Tel: +380 44 235 4371. Fax: +380 44 286 2467.

ACKNOWLEDGMENTS

Grant Agencies (Slovakia: VEGA 1/1005/09 and 1/0052/11, APVV-0202-10, and VVCE 0004-07) are acknowledged for financial support. High-field EPR and Mössbauer spectra were taken at the NHMFL, which is funded by the NSF through the Cooperative Agreement DMR-0654118, the State of Florida, and the Department of Energy. The Mössbauer instrument was purchased using the User Collaboration Grant Program UCGP 5064 funds awarded to A.O. We also thank Dr. Dmytro S. Nesterov for helpful discussions.

REFERENCES

(1) (a) McInnes, E. J. L.; Piligkos, S.; Timco, G. A.; Winpenny, R. E. P. *Coord. Chem. Rev.* **2005**, *249*, 2577. (b) Thompson, L. K. *Coord. Chem. Rev.* **2002**, *233*−*234*, 193.

(2) Kurtz, D. M. Jr. *Chem. Rev.* **1990**, *90*, 585. Lohr, T. M. *Iron Carriers and Iron Proteins*; VCH: Weinheim, Germany, 1989. Pavlosky, M. A.; Solomon, E. I. *J. Am. Chem. Soc.* **1994**, *116*, 11610. Holmes, M. A.; Stenkamp, R. E. *J. Mol. Biol.* **1991**, *220*, 723. Sheriff, S.; Hendrickson, W. A.; Smith, J. L. *J. Mol. Biol.* **1987**, *197*, 273.

(3) Shiemke, A. K.; Loehr, T. M.; Sanders-Loehr, J. *J. Am. Chem. Soc.* **1986**, *108*, 2437. Rosenzweig, A. C.; Frederick, C. A.; Lippard, S. J.; Nordlund, P. *Nature* **1993**, *366*, 537. Anderson, K. K.; Froland, W. A.; Lee, S.-K.; Lipscomb, J. D. *New J. Chem.* **1991**, *15*, 411. Green, J.; Dalton, H. *J. Biol. Chem.* **1989**, *264*, 17698. Nordlund, P.; Eklund, H. *J. Mol. Biol.* **1993**, *232*, 123.

(4) Strater, N.; Klabunde, T.; Tucker, P.; Witzel, H.; Krebs, B. *Science* **1995**, *268*, 1489.

(5) Kissinger, C. R.; Parge, H.; Knighton, D. R.; Lewis, C. T.; Pelletier, L. A.; Tempczyk, A.; Kalish, V. J.; Tucker, K. D.; Showalter, R. E.; Moomaw, E. W.; Gastinel, L. N.; Habuka, N.; Chen, X.; Maldonado, F.; Barker, J. E.; Bacquet, R.; Villafranca, J. E. *Nature (London)* **1995**, *378*, 641.

(6) Egloff, M-P.; Cohen, P. T. W.; Reinemer, P.; Barford, D. *J. Mol. Biol.* **1995**, *254*, 942.

(7) Bagai, R.; Datta, S.; Betancur-Rodriguez, A.; Abboud, K. A.; Hill, S.; Christou, G. *Inorg. Chem.* **2007**, *46*, 4535. Bagai, R.; Abboud, K. A.; Christou, G. *Inorg. Chem.* **2007**, *46*, 5567. Jones, L. F.; Brechin, E. K.; Collison, D.; Helliwell, M.; Mallah, T.; Piligkos, S.; Rajaraman, G.; Wernsdorfer, W. *Inorg. Chem.* **2003**, *42*, 6601. Canada-Vilalta, C.; O'Brien, T. A.; Brechin, E. K.; Pink, M.; Davidson, E. R.; Christou, G. *Inorg. Chem.* **2004**, *43*, 5505. Gatteschi, D.; Sessoli, R.; Cornia, A. *Chem. Commun.* **2000**, 725. Powell, G. W.; Lancashire, H. N.; Brechin, E. K.; Collison, D.; Health, S. L.; Mallah, T.; Wernsdorfer, W. *Angew. Chem., Int. Ed.* **2004**, *43*, 5772. Benelli, C.; Cano, J.; Journaux, Y.; Sessoli, R.; Solan, G. A.; Winpenny, R. E. P. *Inorg. Chem.* **2001**, *40*, 188. Oshio, H.; Hoshino, N.; Ito, T.; Nakano, M.; Renz, F.; Gütlich, P. *Angew. Chem., Int. Ed.* **2003**, *42*, 223. Barra, A. L.; Caneschi, A.; Cornia, A.; Fabrizi de Biani, F.; Gatteschi, D.; Sangregorio, C.; Sessoli, R.; Sorace, L. *J. Am. Chem. Soc.* **1999**, *121*, 5302. Oshio, H.; Hoshino, N.;

Ito, T. *J. Am. Chem. Soc.* **2000**, *122*, 12602. Goodwin, J. C.; Sessoli, R.; Gatteschi, D.; Wernsdorfer, W.; Powell, A. K.; Heath, S. L. *J. Chem. Soc., Dalton Trans.* **2000**, 1835.
(8) Garnovskii, A. D.; Kharissov, B. I. *Direct Synthesis of Coordination and Organometallic Compounds*; Elsevier Science: Amsterdam, The Netherlands, 1999. Kokozay, V. N.; Shevchenko, D. V. *Mater. Sci.-Pol.* **2005**, *23*, 287.
(9) Nesterov, D. S.; Kokozay, V. N.; Jezierska, J.; Pavlyuk, O. V.; Boča, R.; Pombeiro, A. J. L. *Inorg. Chem.* **2011**, *50*, 4401. Buvaylo, E. A.; Kokozay, V. N.; Vassilyeva, O. Yu.; Skelton, B. W.; Jezierska, J.; Brunel, L. C.; Ozarowski, A. *Chem. Commun.* **2005**, 4976. Vinogradova, E. A.; Kokozay, V. N.; Vassilyeva, O. Yu.; Skelton, B. W.; Bjernemosee, J. K.; Raithby, P. R. *J. Chem. Soc., Dalton Trans.* **2002**, 4248. Kovbasyuk, L. A.; Vassilyeva, O. Yu.; Kokozay, V. N.; Linert, W.; Skelton, B. W.; Oliver, A. G. *New J. Chem.* **1998**, *22*, 931.
(10) Nikitina, V. M.; Nesterova, O. V.; Kokozay, V. N.; Dyakonenko, V. V.; Shishkin, O. V.; Jezierska, J. *Polyhedron* **2009**, *28*, 1265. Nikitina, V. M.; Nesterova, O. V.; Kokozay, V. N.; Dyakonenko, V. V.; Shishkin, O. V.; Jezierska, J. *Inorg. Chem. Commun.* **2009**, *12*, 101. Shevchenko, D. V.; Kokozay, V. N.; Krasovska, M. V.; Shishkin, O. V. *Inorg. Chem. Commun.* **2008**, *11*, 1209. Nikitina, V. M.; Nesterova, O. V.; Kokozay, V. N.; Goreshnik, E. A.; Jezierska, J. *Polyhedron* **2008**, *27*, 2426. Shevchenko, D. V.; Petrusenko, S. R.; Kokozay, V. N.; Zhigalko, M. V.; Zubatyuk, R. I.; Shishkin, O. V.; Skelton, B. W.; Raithby, P. R. *Inorg. Chim. Acta* **2005**, *358*, 3889.
(11) Sunatsuki, Y.; Motoda, Y.; Matsumoto, N. *Coord. Chem. Rev.* **2002**, *226*, 199. Kojima, M.; Taguchi, H.; Tsuchimoto, M.; Nakajima, K. *Coord. Chem. Rev.* **2003**, *237*, 183. Vigato, P. A.; Tamburini, S. *Coord. Chem. Rev.* **2004**, *248*, 1717.
(12) Hassan, A. K.; Pardi, L. A.; Krzystek, J.; Sienkiewicz, A.; Goy, P.; Rohrer, M.; Brunel, L.-C. *J. Magn. Reson.* **2000**, *142*, 300.
(13) (a) Sheldrick, G. M. *SADABS*; Universität Göttingen: Göttingen, Germany, 2004. (b) Sheldrick, G. M. *Acta Crystallogr., Sect. A* **2008**, *64*, 112.
(14) Cambridge Structural Database (CSD), version 5.31 (Aug 2010). Allen, F. H. *Acta Crystallogr. Sect. B* **2002**, *58*, 380.
(15) (a) Murugesu, M.; Mishra, A.; Wernsdorfer, W.; Abboud, K. A.; Christou, G. *Polyhedron* **2006**, *25*, 613. (b) Mills, D. K.; Hsiao, Y. M.; Farmer, P. J.; Atnip, E. V.; Reibenspies, J. H.; Darensbourg, M. Y. *J. Am. Chem. Soc.* **1991**, *113*, 1421. (c) Verhagen, J. A. W.; Lutz, M.; Spek, A. L.; Bouwman, E. *Eur. J. Inorg. Chem.* **2003**, 3968. (d) Mathur, S.; Veith, M.; Rapalaviciute, R.; Shen, H.; Goya, G. F.; Filho, W. L. M.; Berquo, T. S. *Chem. Mater.* **2004**, *16*, 1906.
(16) Boudalis, A. K.; Dahan, F.; Bousseksou, A.; Tuchagues, J.-P.; Perlepes, S. P. *Dalton Trans.* **2003**, 3411. Burger, J.; Klufers, P. *Z. Anorg. Allg. Chem.* **1997**, *623*, 1547. Taguchi, T.; Stamatatos, T. C.; Abboud, K. A.; Jones, C. M.; Poole, K. M.; O'Brien, T. A.; Christou, G. *Inorg. Chem.* **2008**, *47*, 4095.
(17) Nesterov, D. S.; Kokozay, V. N.; Dyakonenko, V. V.; Shishkin, O. V.; Jezierska, J.; Ozarowski, A.; Kirillov, A. M.; Kopylovich, M. N.; Pombeiro, A. J. L. *Chem. Commun.* **2006**, 4605.
(18) Winpenny, R. E. P. *Compr. Coord. Chem. II* **2004**, *7*, 125.
(19) Luo, F.; Zheng, J.-m.; Kurmoo, M. *Inorg. Chem.* **2007**, *46*, 8448.
(20) (a) Boča, R. *Theoretical Foundations of Molecular Magnetism*; Elsevier: Amsterdam, The Netherlands, 1999. (b) Boča, R. *Program POLYMAGNET-08*; Slovak University of Technology: Bratislava, Slovakia, 2008.
(21) (a) Ozarowski, A. *Inorg. Chem.* **2008**, *47*, 9760. (b) Ozarowski, A.; Szymańska, I. B.; Muzioł, T.; Jezierska, J. *J. Am. Chem. Soc.* **2009**, *131*, 10279. (c) Semenaka, V. V.; Nesterova, O. V.; Kokozay, V. N.; Dyakonenko, V. V.; Zubatyuk, R. I.; Shishkin, O. V.; Boča, R.; Jezierska, J.; Ozarowski, A. *Inorg. Chem.* **2010**, *49*, 5460.
(22) (a) Owen, J. *J. Appl. Phys.* **1961**, *32*, 213S. (b) Abragam, A.; Bleaney, B. *Electron Spin Resonance of Transition Ions*; Clarendon Press: London, 1970. (c) Bencini, A.; Gatteschi, D. *EPR of Exchange Coupled Systems*; Springer Verlag: Berlin, 1990. (d) Okamura, M. Y.; Hoffman, B. M. *J. Chem. Phys.* **1969**, *51*, 3128. Ozarowski, A.; McGarvey, B. R.; Drake, J. E. *Inorg. Chem.* **1995**, *34*, 5558.
(23) Gorun, S. M.; Lippard, S. J. *Inorg. Chem.* **1991**, *30*, 1625.